Ballooning theory of the second kind—two dimensional tokamak modes

T. Xie,[1] Y. Z. Zhang,[2] S. M. Mahajan,[3] and A. K. Wang[1]
[1]*Southwestern Institute of Physics, Chengdu, China*
[2]*Center for Magnetic Fusion Theory, Chinese Academy of Sciences, Hefei, China*
[3]*Institute for Fusion Studies, University of Texas at Austin, Austin, Texas 78712, USA*

(Received 2 February 2012; accepted 24 May 2012; published online 10 July 2012)

The 2-D ballooning transform, devised to study local high toroidal number (n) fluctuations in axisymmetric toroidal system (like tokamaks), yields a well-defined partial differential equation for the linear eigenmodes. In this paper, such a ballooning equation of the second kind is set up for ion temperature gradient driven modes pertinent to a 2-D non-dissipative fluid plasma; the resulting partial differential equation is numerically solved, to calculate the global eigenvalues, and the 2-D mode structure is presented graphically along with analytical companions. The radial localization of the mode results from translational symmetry breaking for growing modes and is a vivid manifestation of spontaneous symmetry breaking in tokamak physics. The eigenmode, poloidally ballooned at $\vartheta = \pm\pi/2$, is radially shifted from associated rational surface. The global eigenvalue is found to be very close to the value obtained in 1-D parameterized ($\lambda = \mp\pi/2$) case. The 2-D eigenmode theory is applied to estimate the toroidal seed Reynolds stress [Y. Z. Zhang, Nucl. Fusion Plasma Phys. **30**, 193 (2010)]. The solution obtained from the relatively simplified ballooning theory is compared to the solution of the basic equation in original coordinate system (evaluated via FFTs); the agreement is rather good. © *2012 American Institute of Physics*. [http://dx.doi.org/10.1063/1.4731724]

I. INTRODUCTION

The late 1970s witnessed the emergence of the conventional ballooning transform (the ballooning theory of first kind (BM-I)) as a tool to solve the 2-D local eigenvalue problem for high toroidal number (n) in axisymmetric toroidal system like tokamaks.[1–3] The new methodology reduced the intrinsic 2-D eigenmode equation to a much simpler 1-D ballooning equation; the feat was accomplished by exploiting the approximate (to the lowest order in the small parameter $1/\sqrt{n}$) translational invariance or the "ballooning symmetry" of the original system. In this formalism, the 2-D toroidal mode, radially localized at a rational surface, is also found to be poloidally localized at either $\vartheta = 0$ or $\vartheta = \pi$. As a result, it admits the up-down symmetry in the poloidal cross section. However, the BM-I analysis is valid only if a well-defined solvability condition is satisfied, and this condition puts restrictions on the mode structure that was, initially, believed to exist only at a given radial position.[4] For a complex system (including non-dissipative ones away from marginal stability (throughout this paper, the complex BM-II always refers to including the non-dissipative system having finite growth rate as well as the dissipative system)), the solvability condition consists of two equations and results in a more stringent constraint for the occurrence of BM-I.[5,6]

While the existence of another type of solution different from BM-I was anticipated since early 1980s,[7,8] the ballooning theory of the second kind (BM-II) was developed only in early 1990s.[9–16] The main features of BM-II, in contrast to BM-I, can be summarized as follows: (a) no restriction due to solvability condition implying that the 2-D toroidal mode may occur at all radii; (b) the poloidal structure can only be localized at $\vartheta = \pi/2$ (or $\vartheta = -\pi/2$); and (c) no up-down symmetry in the poloidal plane.

Both BM-I and BM-II begin by subjecting the original mode equation to the 2-D ballooning transform[5]

$$\phi_l(x) = \frac{1}{2\pi}\int_{-\pi}^{\pi} d\lambda \int_{-\infty}^{+\infty} dk e^{ik(x-l)-i\lambda l}\varphi(k,\lambda), \qquad (1)$$

a mathematically proper transform with a unique inverse. The LHS of Eq. (1), $\phi_l(x)$, denotes the mode in the physical representation (x, l) where x is the radial variable and l labels the discrete poloidal variable (see Eqs. (6) and (8) for detail). The variables x and l enter the exponent as $x - l$ implying the translational invariance first noted by Lee and Van Dam.[2] The transformed potential $\varphi(k, \lambda)$ is a function of two continuous variables $k \in (-\infty, \infty)$ and $\lambda \in [-\pi, \pi]$; The second variable λ "extends" the parameter $\lambda(\vartheta_0)$ in Lee-Van Dam (Connor, Hastie, and Taylor) representation. Both these representations are special cases in which $\phi(k, \lambda)$ is a Dirac δ-function $\delta(\lambda - \lambda_0)$. The explicit λ-dependence of $\phi(k, \lambda)$ reminds us that the localization in λ, the second dimension, is to be determined (or no localization at all as in the toroidal Alfvén eigenmode mode[9,13,17–20]) *a post-priori* as the solution of the partial differential equation.

Invoking Eq. (1), the large n, 2-D mode equation (for $\phi_l(x)$) transforms to the 2-D ballooning equation

$$\left(L_0 + \frac{iL_1}{n}\frac{\partial}{\partial\lambda} + \frac{L_2}{n^2}\frac{\partial^2}{\partial\lambda^2} + \cdots - \Omega\right)\phi(k,\lambda) = 0, \qquad (2)$$

where, the operators L_0, L_1, L_2, … may contain $\partial/\partial k$, k, λ but not $\partial/\partial\lambda$, and Ω is the global eigenvalue associated with the 2-D ballooning equation. The ballooning operator L_0 embodies the approximate translational symmetry ($x \to x + 1$, $l \to l + 1$) of the original 2-D eigenmode equation and is invariant under the combined parity (CP)

operation ($k \to -k$, $\lambda \to -\lambda$). It must be emphasized that the asymptotic expansion parameter of Eq. (2) is not $1/n$, but the operator $(1/n)\partial/\partial\lambda$, implying that the validity of the asymptotic expansion depends on the mode structure in the λ space. In other words, for a consistent asymptotic analysis, the 2-D eigenfunction $\phi(k,\lambda)$ must satisfy the condition $(1/n)\partial \ln\phi(k,\lambda)/\partial\lambda \ll 1$.

The lowest order limit of Eq. (2) ($(1/n)\partial/\partial\lambda \ll 1$) is the well-known 1-D ballooning equation

$$[L_0 - \Omega(\lambda)]\chi(k,\lambda) = 0. \tag{3}$$

Notice that to the lowest order λ is merely a parameter, and $\chi(k,\lambda)$ is defined to be the eigenfunction of the operator L_0 associated with the λ-parameterized (not global) eigenvalue $\Omega(\lambda)$.

Let us, now, seek a 2-D solution of the form

$$\varphi(k,\lambda) = \psi(\lambda)\chi(k,\lambda). \tag{4}$$

Multiplying by the complex conjugate of χ and integrating over k (on both sides of Eq. (2)) to annihilate one dimension, one obtains the equation for $\psi(\lambda)$

$$\left(\frac{i\overline{L}_1}{n}\frac{\partial}{\partial\lambda} + \frac{\overline{L}_2}{n^2}\frac{\partial^2}{\partial\lambda^2} - [\Omega - \Omega(\lambda)]\right)\psi(\lambda) + \cdots = 0, \tag{5}$$

where, $\overline{L}_j \equiv \int_{-\infty}^{\infty} dk\chi^* L_j\chi / \int_{-\infty}^{\infty} dk\chi^*\chi$ $(j = 1,2,\cdots)$ and χ^* is the complex conjugate of χ. For a λ-localized ballooning solution, $\psi(\lambda)$ varies more rapidly in λ than $\chi(k,\lambda)$. Specifically, it means that $\partial \ln\psi/\partial\lambda \gg \partial \ln\chi/\partial\lambda$ (noting that $\partial \ln\chi/\partial\lambda \sim O(1)$). On the other hand, the truncation of asymptotic series requires $\xi \equiv (1/n)\partial \ln\psi/\partial\lambda \ll 1$. As mentioned earlier,[15] the small parameter $\varepsilon \approx 1/\sqrt{n}$ provides a consistent ordering for the above two conditions being satisfied simultaneously. It means that ξ becomes $1/\sqrt{n}$ only for the localized mode ($\partial \ln\psi/\partial\lambda \sim O(\sqrt{n})$). Existence of such localized $\psi(\lambda)$ is the characteristic of the ballooning symmetry breaking.

For BM-I, the first-order perturbation in Eq. (5) is assumed to give no contribution, i.e., $\overline{L}_1 = 0$ (the solvability condition). Owing to the CP conservation of both the 1-D ballooning and the 2-D equation (up to second order in $(1/n)\partial/\partial\lambda$), the mode structure $\psi(\lambda)$ is localized at $\lambda_0 = 0$ or π, which is equivalent to the poloidal angel $\vartheta = 0$ or π. The global eigenvalue Ω is close to the local eigenvalue (the λ-parameterized eigenvalue $\Omega(\lambda)$ at $\lambda_0 = 0$ or π) with only a second-order correction, $\Omega - \Omega(\lambda_0) \sim O(\varepsilon^2)$. As mentioned earlier, the meaning of the solvability condition needs to be examined; this can be challenging in general but particularly so for complex systems.[5,6]

For BM-II, in contrast, the second-order terms in Eq. (5) are neglected while $\overline{L}_1$ remains non zero. As a result, the CP symmetry, conserved for the 1-D ballooning equation, is violated in the second dimension for the BM-II equation. For a complex BM-II, this violation leads to the localization of the mode structure at $\lambda_0 = \pi/2$ or $-\pi/2$ (corresponding to the poloidal angel $\vartheta = -\pi/2$ or $\pi/2$). The global eigenvalue will be shown correct to the 2nd order of the local eigenvalue: $\Omega(\lambda_0)$. In order for BM-II to have a poloidal localization, the system does not need to be necessarily dissipative. As pointed out in Refs. 15, 16, and 21, the equilibrium free energy, driving the instability, could be sufficient to warrant such localization. Because it also leads to the breakdown of the up-down symmetry of mode structure, the instability driven asymmetry is an example of spontaneous symmetry breaking.[21]

For both BM-I and the complex BM-II, it is the translational symmetry breaking of the 2-D ballooning equation that results in the poloidal as wells as radial localization of mode structure. The conservation of CP for BM-I leads to the radial symmetry of the eigenmode. However, the CP symmetry breaking of the complex BM-II causes the radial asymmetry of mode around the associated rational surface. This radial asymmetry is found to yield the finite seed parallel Reynolds stress (Ref. 21) offering an alternative turbulence driven mechanism to those proposed by other theories.[22–30] The parallel Reynolds stress is shown to be zero for the slab modes in absence of equilibrium flows and electric fields.[31]

For reader's convenience, a few remarks are in order with regard to various concepts in literature originating in different symmetry breaking terms,[15,21] namely ballooning symmetry breaking, radial symmetry breaking, up-down symmetry breaking, combined parity symmetry breaking, and spontaneous symmetry breaking. The two terms "symmetry breaking" and "symmetry violation" are used here interchangeably.

The ballooning symmetry is, technically, the (combined) translational invariance as mentioned above. Such symmetries, often, facilitate system analysis—equally significant is the general notion that symmetry breaking imparts interesting properties to the system. Translation invariance, for example, implies no spatial structure (localization, for instance). To create spatial structure, then, one would seek mechanisms that break translational invariance. It is in this context that the ballooning symmetry (and symmetry-breaking) has attracted considerable theoretical attention in tokamak research.

Seeking localization of 2-D high n toroidal modes in tokamaks, the 2-D mode equations have to be "properly" solved. There are leading contenders for the proper solution: BM-I and BM-II-both are particular solutions of the 2-D ballooning equations and are characterized by different reflection symmetries.

Radial symmetry, in the tokamak context, refers to the reflection symmetry of the mode structure with respect to the pertaining rational surface. There exist many one-dimensional (1-D) models where the radial symmetry violation is associated with details of the model—shear flow driven instabilities are an example. It is also widely accepted that without such symmetry violation, toroidal rotation cannot be driven in a 1-D model. That raises a theoretically interesting question—Are even instabilities, associated with such a 1-D mode, excluded from the candidate list that could drive toroidal rotation? By exploring a fluid ion temperature gradient (ITG) model, we demonstrate that the answer is no; instabilities could, indeed, power torioidal rotation.

Up-down symmetry refers to the reflection symmetry of the mode structure with respect to the equatorial surface of the tokamak. Because toroidal rotation does imply up-down symmetry violation, the associated mode structure of the turbulence drive must, necessarily, violate the up-down symmetry.

CP symmetry pertains to the simultaneous reflection in radial and poloidal directions. Mathematically, it corresponds to $k \to -k$, $\lambda \to -\lambda$ in the 2-D ballooning equations and is equivalent to the simultaneous reflection ($x \to -x$, $l \to -l$) in the (x, l) representation. Both the ballooning equation and the BM-I mode conserve CP symmetry. BM-II, however, does not leading to up-down asymmetry. This is the universal or ubiquitous mechanism (regardless of specific modes) of driving not only toroidal but also poloidal Reynolds stress.[15]

The concept of spontaneous symmetry breaking is associated with instability-driven asymmetry. For barely unstable modes in a non-dissipative fluid ITG model, the system is almost real. Such modes are not radially localized, and the asymptotic expansion parameter ξ is not small enough to guarantee the validity of the skewed mode. Even if such modes were to exist, they will not fall into the non-dissipative BM-II class. Therefore, the purposely chosen non-dissipated fluid ITG model is adopted to demonstrate the mechanism of spontaneous symmetry breaking. Such a mechanism may not be even significant in reality when the system is dissipative. The intrinsic dissipation could provide mode localization even for marginally stable BM-II modes.

The rest of this paper is organized as follows. In Sec. II of the paper, a non-dissipative 2-D fluid model, appropriate for demonstrating spontaneous symmetry breaking, is devised for the ion temperature gradient driven mode. The model is then transformed into a 2-D ballooning equation and solved analytically under certain simplifying assumptions. The analysis of Sec. II is verified in Sec. III using a novel, iterative numerical method. The detailed iterative procedure of the numerical method is given in Appendix A. The verification, displayed in graphics for two typical parameter sets A and B, spans the global eigenvalue, the asymptotic condition, and the mode structure. In particular, the verification of the asymptotic condition is displayed graphically by substituting the ballooning solution back into the original mode equation in the x-l representation via fast Fourier transform (FFT). Since the seed parallel Reynolds stress is the natural consequence of the skewed mode structure of BM-II, its calculation in 2-D ballooning representation is presented in Sec. IV. Our detailed calculation confirmed the earlier prediction that the seed parallel Reynolds stress reverses sign when the magnetic shear measure equals unity.[21] We have also explored the complex issues one faces when an attempt is made to apply the current work to experimental observations.[32–35] Major conclusions of this paper are summarized in Sec. V. The analytical solution of ballooning equation for arbitrary λ is also found very useful for comparison between analytical and numerical results. It is given in Appendix B.

II. MODEL EQUATION AND ANALYTIC SOLUTION IN BALLOONING REPRESENTATION

In this section, drawn heavily from Ref. 21, we investigate a non-dissipative fluid ITG model pertaining to an axisymmetric, large-aspect-ratio torus with concentric, circular magnetic surfaces. In the quasitoroidal coordinates (r, ϑ, ζ) that correspond, respectively, to the minor radial, poloidal, and toroidal directions, the toroidal mode that is localized at the rational surface r_0 is represented by

$$\varphi_n(r,\vartheta,\zeta) = e^{-i\omega t + in\zeta - im\vartheta} \sum_l \varphi_l(r) e^{-il\vartheta}, \tag{6}$$

where n is the toroidal mode number, $m = nq(r_0)$, and the integer l labels the sidebands coupled to the central Fourier mode m. The 2-D fluid ITG eigenmode equation is derived (zero equilibrium radial electric field and flow) from the three lowest order ion fluid transport equations, namely particle, momentum, and energy conservation law. In this derivation, we also use the adiabatic electron response and quasi-neutrality condition, and obtain [36,37]

$$\left[\rho_s^2 \nabla_\perp^2 - \frac{c_s^2}{\omega^2}\nabla_\parallel^2 - \frac{\omega - \hat{\omega}_{*e}}{\omega + \hat{\omega}_{*i}} - \frac{2\hat{\omega}_{de}}{\omega}\right]\phi_n(r,\vartheta,\zeta) = 0, \tag{7}$$

where $\nabla_\perp^2 \equiv \partial^2/\partial r^2 + (1/r^2)\partial^2/\partial\vartheta^2$, $\nabla_\parallel \equiv \mathbf{b}\cdot\nabla = (1/qR)[\partial/\partial\vartheta + q(r)\partial/\partial\zeta]$, $\rho_s \equiv \sqrt{m_i T_e}/eB$, $c_s \equiv \sqrt{T_e/m_i}$, $\hat{\omega}_{*e} \equiv \omega_{*e}\quad (in q)\partial/\partial\vartheta$, $\omega_{*e} \equiv (k_\vartheta T_e/eB)(d\ln n_0/dr)$, $\hat{\omega}_{*i} \equiv \omega_{*i}(i/nq)\quad \partial/\partial\vartheta$, $\omega_{*i} \equiv (k_\vartheta T_i/eB)(d\ln p_i/dr)$, $\hat{\omega}_{de} \equiv \omega_{de}(i/nq)(r\sin\vartheta\partial/\partial r + \cos\vartheta\partial/\partial\vartheta)$, $\omega_{de} \equiv -k_\vartheta T_e/eBR$, and $k_\vartheta \equiv m/r_0$. Additionally, T_e is the electron temperature, n_0 is the plasma density in equilibrium, T_i and p_i are the ion temperature and pressure respectively, e is the unit charge, B is the magnetic field, and R is the major radius; all physical quantities are evaluated at $r = r_0$ except for $q(r)$.

Introducing new radial variables $x \equiv k_\vartheta \hat{s}(r - r_0)$, where $\hat{s} \equiv d\ln q(r)/d\ln r$, and substituting Eq. (6) into Eq. (7) yields the model equation in (x, l) representation. At this stage, we further restrict our model by using an ad hoc symmetry breaking term, basically, arising from the $\partial/\partial\vartheta$ contained in $\hat{\omega}_{*i}$. The 2-D model equation in (x, l) representation (up to first order in l/m), then, reads as

$$\left\{(k_\vartheta\rho_s\hat{s})^2\frac{d^2}{dx^2} + \frac{\omega_s^2}{\omega^2}(x-l)^2 - \frac{1+(k_\vartheta\rho_s)^2 + (\omega_{*i}/\omega)\left[(k_\vartheta\rho_s)^2 - \omega_{*e}/\omega_{*i}\right]}{1+(\omega_{*i}/\omega)}\right.$$
$$\left. + \frac{1+(k_\vartheta\rho_s)^2 + (\omega_{*i}/\omega)\left[(k_\vartheta\rho_s)^2 - \omega_{*e}/\omega_{*i}\right]}{(1+\omega_{*i}/\omega)^2}\frac{\omega_{*i}}{\omega}\frac{l}{m}\right\}\varphi_l(x) - \frac{\omega_{de}}{\omega}\left[\left(1+\hat{s}\frac{d}{dx}\right)\varphi_{l+1}(x) + \left(1-\hat{s}\frac{d}{dx}\right)\varphi_{l-1}(x)\right] = 0. \tag{8}$$

This is the model equation that we shall study to explore the content of the ballooning theory of second kind. The substitutions[5]

$$\frac{d}{dx} \to ik,\ (x-l) \to i\frac{\partial}{\partial k},\quad l \to -i\frac{\partial}{\partial \lambda},$$
$$\varphi_{l\pm 1}(x) \to e^{\mp i(k+\lambda)}\phi(k,\lambda) \tag{9}$$

transform Eq. (8) into the 2-D ballooning equation of the second kind

$$\left(L_0 + \frac{iL_1}{n}\frac{\partial}{\partial \lambda} - \Omega\right)\phi(k,\lambda) = 0, \tag{10}$$

where

$$L_0 = \frac{1}{\eta^2}\frac{\partial^2}{\partial k^2} + \eta^2 k^2 - \frac{2q}{\hat{s}}[\cos(k+\lambda) + k\hat{s}\sin(k+\lambda)], \tag{11}$$

$$L_1 = \frac{1}{\hat{s}\varepsilon_n}\frac{\omega_{*i}}{\omega_{*e}}\frac{1 + (k_\vartheta \rho_s)^2 + \omega_{*i}\left[(k_\vartheta\rho_s)^2 - \omega_{*e}/\omega_{*i}\right]/\omega}{(1+\omega_{*i}/\omega)^2}, \tag{12}$$

$$\Omega = -\frac{q}{\hat{s}\varepsilon_n}\frac{\omega}{\omega_{*e}}\frac{1 + (k_\vartheta \rho_s)^2 + \omega_{*i}\left[(k_\vartheta\rho_s)^2 - \omega_{*e}/\omega_{*i}\right]/\omega}{1+\omega_{*i}/\omega}, \tag{13}$$

and $\eta^2 \equiv \omega k_\vartheta \rho_s \hat{s}/\omega_s$, $\varepsilon_n \equiv L_n/R$, $L_n \equiv (d\ln n_0/dr)^{-1}$, and $\omega_s \equiv c_s/qR$. Equation (10) is the precise BM-II version of Eq. (2) for the physical model Eq. (8).

In order to solve 2-D BM-II, Eq. (10), we begin with the ballooning equation

$$\left\{\frac{1}{\eta^2}\frac{\partial^2}{\partial k^2} + \eta^2 k^2 - \frac{2q}{\hat{s}}[\cos(k+\lambda) + k\hat{s}\sin(k+\lambda)] - \Omega(\lambda)\right\}\chi(k,\lambda) = 0 \tag{14}$$

with the evanescent boundary condition at large $|k|$. Substituting Eq. (4) into Eq. (10) and invoking the annihilation procedure, we obtain the differential equation in λ (the second dimension)

$$\frac{i\overline{L}_1}{n}\left(\frac{d\ln\psi(\lambda)}{d\lambda} + \overline{\frac{\partial \ln\chi}{\partial\lambda}}\right) - [\Omega - \Omega(\lambda)] = 0 \tag{15}$$

with $\psi(\lambda)$ obeying periodic boundary condition. In Eq. (15),

$$\overline{L}_1 \equiv \frac{\int_{-\infty}^{\infty} dk \chi^* L_1 \chi}{\int_{-\infty}^{\infty} dk \chi^* \chi}. \tag{16}$$

Consistent with the ordering of the asymptotic theory, the term $\overline{\frac{\partial \ln\chi}{\partial\lambda}}$ can be neglected in Eq. (15) as long as the condition $\partial \ln\chi/\partial\lambda \ll d\ln\psi/d\lambda$ is satisfied. Eq. (15) is, then, reduced to

$$\frac{i\overline{L}_1}{n}\frac{d\ln\psi(\lambda)}{d\lambda} - [\Omega - \Omega(\lambda)] = 0. \tag{17}$$

Because of the CP conservation of the ballooning operator, the λ-parameterized eigenvalue $\Omega(\lambda)$ can be approximated by a truncated Fourier series in $\cos p\lambda$ ($p = 0, 1, 2, \ldots$), e.g.,

$$\Omega(\lambda) = c_0 + c_1\cos\lambda + \cdots. \tag{18}$$

The set of Eqs. (14) and (17) constitutes the starting point of the numerical solution as presented in Sec. III. The analytical solution, however, is also found feasible by assuming that only the first two terms in Eq. (18) are significant for localized modes, i.e.,

$$\Omega(\lambda) = c_0 + c_1\cos\lambda. \tag{19}$$

This approximation is found plausible in our numerical explorations in Sec. III. Substituting Eq. (19) into Eq. (17), then integrating over λ, we obtain the eigenvalue $\Omega = c_0$ owing to the periodic boundary condition on $\psi(\lambda)$. Then, $\psi(\lambda)$ is solved to be

$$\psi(\lambda) = \psi(0)e^{in\mu\sin\lambda}, \tag{20}$$

where $\mu \equiv c_1/\overline{L}_1$. This simple expression is obtained because in our model, L_1 is independent of λ. If μ is complex and finite (not too small imaginary part), $\psi(\lambda)$ becomes localized either at $\pi/2$ ($\mathrm{Im}\,\mu < 0$) or at $-\pi/2$ ($\mathrm{Im}\,\mu > 0$) in the limit of large n. The asymptotic expansion parameter turns out to be

$$\xi \equiv \frac{1}{n}\frac{\partial\ln\psi}{\partial\lambda} \sim \sqrt{\frac{|\mathrm{Im}\mu|}{n}} \ll 1 \tag{21}$$

and $\psi(\lambda)$ has a width

$$\triangle\lambda \equiv \frac{1}{\sqrt{n|\mathrm{Im}\mu|}} \ll 1. \tag{22}$$

Putting it all together, the condition for the asymptotic theory to be valid, works out to be

$$\frac{1}{n} \ll |\mathrm{Im}\,\mu| \ll n. \tag{23}$$

Now, we are able to analytically solve the ballooning equation in certain parameter ranges by adopting the standard method in literature (Ref. 15 and references cited herein). At $\lambda_0 = \sigma_\lambda\pi/2$ ($\sigma_\lambda = 1$ for $\mathrm{Im}\,\mu < 0$ and $\sigma_\lambda = -1$ for $\mathrm{Im}\,\mu > 0$ (this can be uniformly expressed $\sigma_\lambda = -\mathrm{sgn}(\mathrm{Im}\mu)$ and termed "localization rule")), the ballooning equation (Eq. (14)) becomes

$$\left[\frac{1}{\eta^2}\frac{\partial^2}{\partial k^2} + V(k) - \Omega(\lambda)\right]\chi\left(k, \sigma_\lambda\frac{\pi}{2}\right) = 0, \tag{24}$$

where $V(k) \equiv \eta^2 k^2 - \sigma_\lambda (2q/\hat{s})[k\hat{s}\cos k - \sin k]$. It is important to note that the ballooning operator acquires maximal parity violation at $\lambda_0 = \sigma_\lambda \pi/2$ in k space. This is in contrast to the conventional ballooning operator that conserves the k parity. Expanding $V(k)$ at k_* defined by $\partial V(k)/\partial k = 0$, we obtain

$$k_* = \sigma_\lambda \frac{q}{\eta^2 \hat{s}}[(\hat{s}-1)\cos k_* - k_* \hat{s} \sin k_*] \tag{25}$$

and the mode structure $\chi(k, \sigma_\lambda \pi/2)$ for large η^2

$$\chi\left(k, \sigma_\lambda \frac{\pi}{2}\right) = e^{i\eta^2 (k-k_*)^2/2}. \tag{26}$$

It is important to note that k_* is a measure of the radial asymmetry of the mode. In the physical space, Eq. (26) reads

$$\overline{\chi}\left(x-l, \sigma_\lambda \frac{\pi}{2}\right) = \sqrt{\frac{2\pi i}{\eta^2}} e^{ik_*(x-l) - i(x-l)^2/(2\eta^2)}. \tag{27}$$

The mode structure given by Eq. (27) retains the translational symmetry, but violates CP conservation. The latter yields a radial symmetry breaking in the "slab" limit ($l \to 0$),

$$\overline{\chi}\left(x, \sigma_\lambda \frac{\pi}{2}\right) = \sqrt{\frac{2\pi i}{\eta^2}} e^{ik_* x - ix^2/(2\eta^2)}. \tag{28}$$

In a sense, it can be called the modified (by toroidicity) slab mode.[21]

Substituting the analytic form of the mode (consisting of Eq. (27) for ballooning base, and Eq. (20) for fast λ modulation) back in the 2-D ballooning representation Eq. (1), and, in turn, into the local mode representation Eq. (6), we obtain the 2-D mode structure in the physical space,

$$\varphi_n(x, \vartheta, \zeta) = \sqrt{\frac{1}{2\pi n|\mu|}} e^{in\zeta - im\vartheta} \sum_l \overline{\chi}(x-l, \sigma_\lambda \pi/2) e^{i\sigma_\lambda [n\mu + l^2/(2n\mu) - l(\sigma_\lambda \vartheta + \pi/2)] + i3\pi/4 - i\vartheta_0/2}, \tag{29}$$

where ϑ_0 is the phase of μ. Equation (29), valid in large n limit, is derived by integrating over λ via the saddle point method. For the finite Im μ, the second term in the exponent of Eq. (29), per the "localization rule," results in rapid decay for $l > \bar{l}$, where $\bar{l}$ is the ballpark number of the influential sidebands

$$\bar{l} \equiv |\mu| \sqrt{\frac{n}{|\mathrm{Im}\mu|}} \ll m. \tag{30}$$

Equation (29) suggests that the mode is poloidally localized at $\vartheta = -\sigma_\lambda \pi/2$ in the large n limit.

Note that for the model equation, where $\overline{L}_1$ is independent of λ, the global eigenvalue is readily obtained by integrating Eq. (17). Its value is thus found very close to that of the local one, since $\cos(\sigma_\lambda \pi/2) = 0$. In general, $\overline{L}_1$ could depend on λ. In that case, Eq. (17) should be divided by $\overline{L}_1$ before doing integration over λ. The global eigenvalue could be slightly away from the local one. The λ-dependency of $\overline{L}_1$ is generally weak, because the dependency can only come into existence through the ballooning solution $\chi(k, \lambda)$ and $\cos\lambda$, $\sin\lambda$, etc. Therefore, the deviation from local eigenvalue is also small. Admittedly, if $\overline{L}_1$ were to cross zero somewhere in λ, the present analysis breaks down, and the theory of BM-II will need to be re-worked.

III. NUMERICAL RESULTS OF GLOBAL EIGENVALUE AND MODE STRUCTURE

One of major goals of this paper was to test and possibly verify the analytic results through detailed numerical calculations. Two typical parameter sets A and B are chosen for the comparison. For the parameter set A, corresponding to the operating conditions on HL-2A ($R = 1.65\,\mathrm{m}$, $a = 0.65\,\mathrm{m}$, $T_e = 1.5\,\mathrm{keV}$, and $B = 2\,\mathrm{T}$), physical parameters of the theory turn out to be: $k_\vartheta \rho_s = 0.6$, $\hat{s} = 1.2$, $q = 1.5$, $\varepsilon_n = -0.1$, $\omega_{*\mathrm{i}}/\omega_{*\mathrm{e}} = 3$, and $n = 60$. The set B, reflecting JET operation ($R = 2.96\,\mathrm{m}$, $a = 1.25\,\mathrm{m}$, $T_e = 3\,\mathrm{keV}$, $B = 3\,\mathrm{T}$), yields the corresponding physical parameters: $k_\vartheta \rho_s = 0.5$, $\hat{s} = 1.5$, $q = 3$, $\varepsilon_n = -0.02$, $\omega_{*\mathrm{i}}/\omega_{*\mathrm{e}} = 6$, and $n = 60$.

In general, a numerical solution of the set of 2-D ballooning equation, Eqs. (14) and (17), is not straightforward, because the parameters contained in the ballooning equation are likely to depend on the mode frequency, which is linked to the global eigenvalue (see Eq. (13), for example). In that case, the coefficients of the equation in first dimension depend on the solution of the equation in second dimension, whose potential $\Omega(\lambda)$, in turn, is the parameterized eigenvalue of the equation in the first dimension. Fortunately, from the analysis in Sec. II, we expect that the global eigenvalue may be well approximated by the local one. This suggests a way to break up the above mentioned entanglement, e.g., by resorting to iteration methods.

The details of the "iterative procedure" are given in Appendix A. In the rest of this section we exhibit, graphically, the numerical solutions of the 2-D ballooning equations and compare them to analytical solutions derived in Sec. II for the parameter sets A and B. The related theoretical parameters are calculated by making use of the global eigenvalues are $\omega/|\omega_{*i}| = 0.108 + 0.0894i$, $\mu = -0.136 - 3.65i$, $\bar{l} = 14.8$, $\eta^2 = 2.10 + 1.74i$, $\sigma_\lambda = 1$ for the set A, and $\omega/|\omega_{*i}| = 0.0706 + 0.0167i$, $\mu = -0.198 - 11.1i$, $\bar{l} = 25.9$, $\eta^2 = 23.8 + 5.64i$, $\sigma_\lambda = 1$ for the set B. Because the validity of the analytical expression of ballooning equation, Eq. (26), gets better for large η^2, one has reason to expect that the analytical results for parameter set B (as compared to set A) should be closer to the numerical solution.

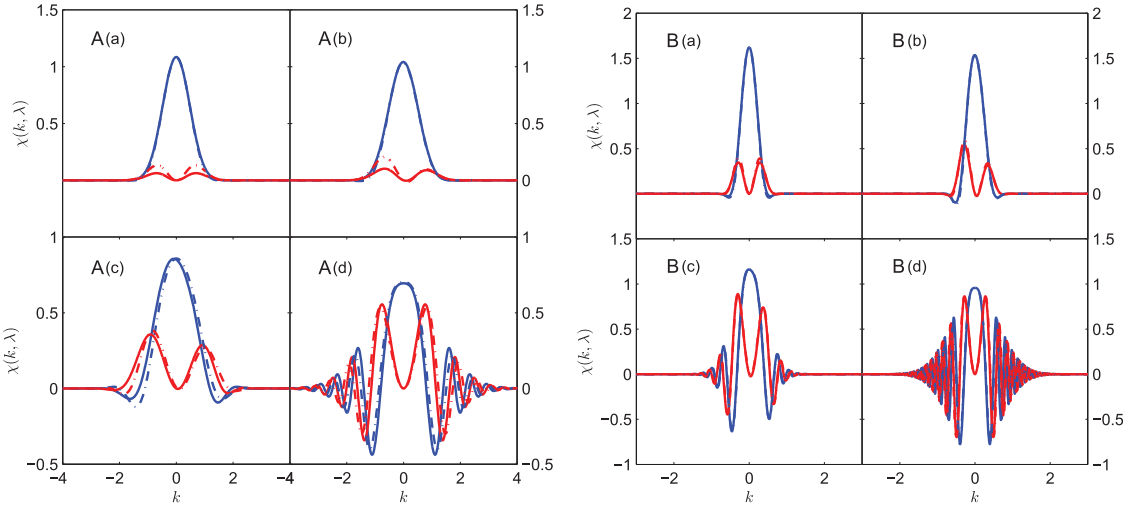

FIG. 1. The real (blue line) and imaginary (red line) parts of ballooning wave functions $\chi(k,\lambda)$ versus k for (a) $\lambda=0$; (b) $\lambda=\pi/4$; (c) $\lambda=\pi/2$; (d) $\lambda=\pi$ for parameter sets A and B. Solid line: numerical solution; dotted-dashed line: analytical solution obtained from Eq. (B4). The parameter sets chosen are $k_\vartheta\rho_s=0.6$, $\hat{s}=1.2$, $q=1.5$, $\varepsilon_n=-0.1$, $\omega_{*i}/\omega_{*e}=3$, $n=60$ for A, and $k_\vartheta\rho_s=0.5$, $\hat{s}=1.5$, $q=3$, $\varepsilon_n=-0.02$, $\omega_{*i}/\omega_{*e}=6$, $n=60$ for B.

The ballooning wave functions $\chi(k,\lambda)$, corresponding to the local eigenvalues, are plotted versus k for $\lambda=0$, $\pi/4$, $\pi/2$, π in Figs. 1A(a)–1A(d) and Figs. 1B(a)–1B(d) for the parameter sets A and B, respectively. The corresponding local eigenvalues are listed in Table I. The numerical results as displayed in Fig. 1 with solid line are obtained from Eqs. (A1), (A3), and (A5) with λ_0 replaced by λ; the dotted-dashed line is the analytical result obtained from Eq. (B4) in Appendix B, the extension of Eq. (26) for arbitrary λ.

Fig. 1 indicates that the parity conservation in k space holds for $\lambda=0$, π, but is violated for $\lambda=\pi/4$, $\pi/2$. The maximal violation is near $\lambda=\pi/2$, and then decreases as λ reaches π. The oscillation of $\chi(k,\lambda)$ for $\lambda=\pi$ is associated with lower growth rate in contrast to $\lambda=0$. Since $\lambda=0$ and $\lambda=\pi$ correspond, respectively, to the good and bad curvature regions of plasma, this result indicates that the bad curvature destabilizes the ITG mode for the given parameter set with less oscillatory mode structure. It is also interesting to mention that while the mode structure is in very good agreement with the analytical formula (Figs. 1B(a)–1B(d)), the analytical result is still acceptable when η^2 is barely above unity (Figs. 1B(a)–1B(d) for parameter set A).

A FORTRAN code is developed to, numerically, solve the global eigenvalue problem of Eqs. (A1)–(A5). All selected numerical results displayed below are obtained from convergent iteration. The wave functions in λ space, $\psi(\lambda)$, are solved and presented in Figs. 2(A) and 2(B) for parameter sets A and B respectively, and compared with the analytic formula in Eq. (20). Numerical solutions in Fig. 2(A) show that the wave function $\psi(\lambda)$ has a width $\Delta\lambda=0.0675$ (defined by Eq. (22)).

TABLE I. The local eigenvalues corresponding to the ballooning wave functions as displayed in Figs. 1(a)–1(d) for both parameter sets A and B.

	Fig. 1A	Fig. 1B
(a) for $\lambda=0$	$\omega/\lvert\omega_{*i}\rvert=0.0755+0.220i$	$\omega/\lvert\omega_{*i}\rvert=0.0455+0.0642i$
(b) for $\lambda=\pi/4$	$\omega/\lvert\omega_{*i}\rvert=0.0749+0.188i$	$\omega/\lvert\omega_{*i}\rvert=0.0472+0.0518i$
(c) for $\lambda=\pi/2$	$\omega/\lvert\omega_{*i}\rvert=0.108+0.0878i$	$\omega/\lvert\omega_{*i}\rvert=0.0704+0.0170i$
(d) for $\lambda=\pi$	$\omega/\lvert\omega_{*i}\rvert=0.214+0.0397i$	$\omega/\lvert\omega_{*i}\rvert=0.110+0.00783i$

It is interesting to observe that the numeric-analytic agreement is excellent for parameter set B, but for the parameter set A the agreement is less good, because the analytical ballooning solution (Eq. (B4)) deviates away from being true for this parameter set ($\eta^2=2.10+1.74i$). It is worth mentioning that for both the parameter sets A and B, Im μ is found to be not "too small" as required by the theory. Also $\psi(\lambda)$ is highly localized at $\lambda=\pi/2$ for Im $\mu<0$, consistent with the theoretical analysis. On the other hand, for Im $\mu>0$, $\psi(\lambda)$ is localized at $\lambda=-\pi/2$. However, for most parameters we explored, Im $\mu<0$ pertains.

The real and imaginary parts of $\Omega(\lambda)$ versus λ are displayed in Figs. 3(A) and 3(B) for parameter sets A and B, respectively. Again $\Omega(\lambda)$ is barely distinguishable from the expression $c_0+c_1\cos\lambda$ used to obtain analytical Eq. (19); The Fourier coefficients up to the 5th harmonics are presented in Table II for both the parameter sets. It also indicates the appropriateness of limiting $\Omega(\lambda)$ to the first harmonic.

Combining the numerical ballooning solution $\chi(k,\lambda)$ and $\psi(\lambda)$ via Eq. (4) and substituting it into Eq. (1), we obtain the 2-D wave functions $\varphi_l(x)$ via FFT. It is displayed in Figs. 4A(a)–4B(a) for parameter sets A and B, respectively, for selected significant sidebands, where solid line stands for $\mathrm{Re}[\varphi_l(x)]$ and dotted-dashed line stands for $\mathrm{Im}[\varphi_l(x)]$. It is seen that $\varphi_l(x)$ decays rapidly with increasing l and can be neglected when $1>\bar{l}$. Therefore, this behavior is in good agreement with analytic expressions given earlier. For example, the decay length $\bar{l}$, defined by Eq. (30), is found to be 14.8 for the parameter set of Fig. 4(A), and the condition $l\ll m$ is numerically verified. The radial positive shift from the associated rational surface ($x=0$) is also seen in Fig. 4.

In order to further compare the numerical results with analytical ones, use is made of Eq. (B6) to calculate $\varphi_l(x)$. The results are displayed in Figs. 4A(b) and 4B(b) for parameter sets A and B, respectively, for a few selected significant sidebands ($l=-4$, 0, 4) only. As expected, the agreement looks better for parameter set B than parameter set A.

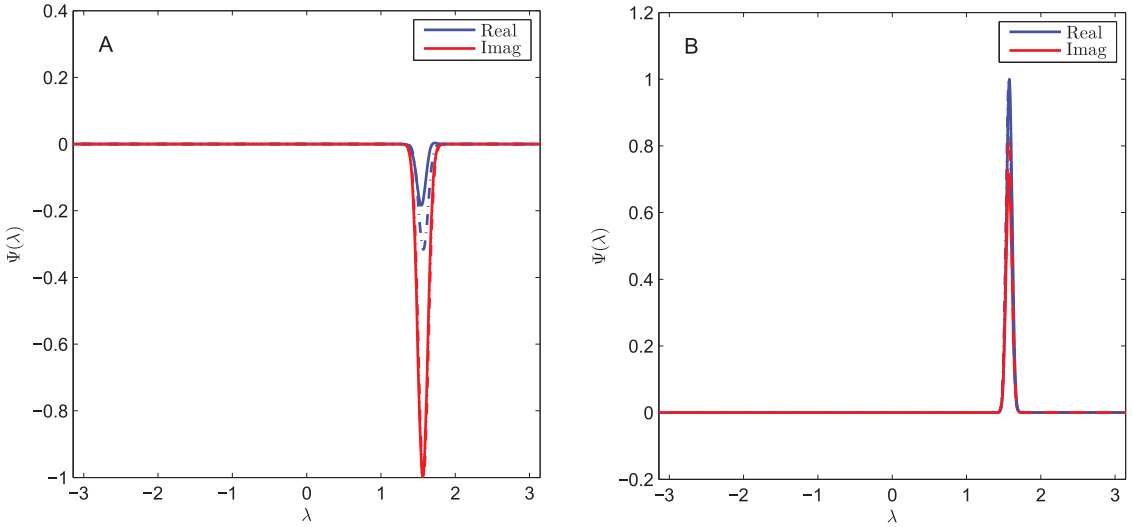

FIG. 2. The localization at $\sigma_\lambda \pi/2$ of second dimensional wave functions $\psi(\lambda)$ for parameter sets A and B. Solid line: numerical solution; dotted-dashed line: analytical solution obtained from Eq. (20).

By making use of the 2-D wave function in (x, l) representation, Eq. (1), and the Poisson formula

$$\sum_l \int_{-\infty}^{\infty} dk e^{-il(k+\lambda+\vartheta)} \chi(k,\lambda) = 2\pi \sum_p \chi(2p\pi - \lambda - \vartheta, \lambda), \tag{31}$$

the mode structure in (x, ϑ) coordinate system, given by Eq. (6), may be expressed as

$$\begin{aligned}\varphi(x,\vartheta) &= e^{-im\vartheta} \sum_l e^{-il\vartheta} \frac{1}{2\pi} \int_{-\pi}^{\pi} d\lambda \psi(\lambda) \int_{-\infty}^{\infty} dk e^{ik(x-l)-i\lambda l} \chi(k,\lambda) \\ &= e^{-im\vartheta} \sum_p \int_{-\pi}^{\pi} d\lambda \psi(\lambda) \chi(2p\pi - \vartheta - \lambda, \lambda) e^{ix(2p\pi-\vartheta-\lambda)}.\end{aligned} \tag{32}$$

Because χ decays rapidly in k space in our numerical calculations, it was found sufficient to include p only up to ± 2.

Figures 5(A) and 5(B) show the real parts of potential contour of the mode structure on a poloidal cross section for the parameter sets of Fig. 4. Use is made of the radial conversion formula $\rho = r_0(1 + x/m\hat{s})/\overline{a}$ to draw the level plot in polar coordinate system. Notice that $\overline{a}$ in the formula is not the minor radius and equals $\overline{a} = 3r_0/2$ in Fig. 5. The blue dotted-dashed line stands for the associated rational surface (r_0). The poloidal localization at $\vartheta = -\pi/2$ is in accordance with the preceding analytical analysis. The radial symmetry breaking can also be seen from the fact that the mode structure is skewed.

Before concluding the section, it is worth checking the "trustworthiness" of our numerical results. We did this by substituting $\varphi_l(x)$ and the global eigenvalue back into the model equation before the ballooning transform, Eq. (8). The accuracy is measured by $F_\varepsilon \equiv \frac{\hat{L}\varphi_l(x)}{\Omega\sqrt{\int \varphi_l^*(x)\varphi_l(x)dx}}$, where $\hat{L}\varphi_l(x)$ is the LHS of Eq. (8). The comparison results are shown for

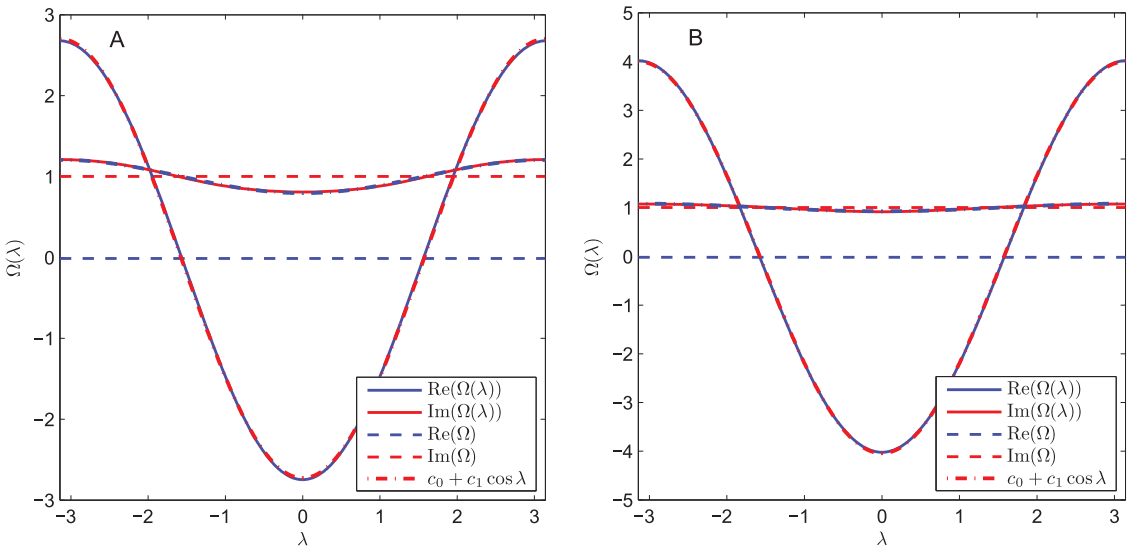

FIG. 3. The real (blue line) and the imaginary (red line) parts of λ-parameterized eigenvalue $\Omega(\lambda)$ versus λ for parameter sets A and B. Solid line: the λ-parameterized eigenvalue $\Omega(\lambda)$; dashed line: the global eigenvalue Ω; dotted-dashed line: $c_0 + c_1 \cos\lambda$.

TABLE II. The Fourier coefficients of $\Omega(\lambda)$ for parameter sets A and B.

Fourier coefficients	Set A	Set B
c_0	$-0.0130 + 1.00i$	$-0.0193 + 1.00i$
c_1	$-2.71 - 0.206i$	$-4.02 - 0.0781i$
c_2	$-0.0234 + 0.00854i$	$0.0176 - 0.00859i$
c_3	$0.00191 + 0.00521i$	$0.00116 - 0.00107i$
c_4	$0.00154 - 0.000570i$	$0.0000726 - 0.000126i$

the following values of the asymptotic expansion parameter defined by Eq. (21): $\xi = 0.247$ in Fig. 6(A) and $\xi = 0.431$ in Fig. 6(B) (or parameter sets A and B, respectively). We find that the precision of the global eigenvalue reaches 10^{-3}, which well satisfies the assumed accuracy ($\sim 1/n$). Thus, such a cross error analysis ensures the validity of the asymptotic approach of ballooning theory for local modes.

IV. SEED PARALLEL REYNOLDS STRESS

The turbulence driven seed parallel Reynolds stress emerges as a natural consequence of the skewed mode structure of BM-II. In this section, we extend the previous analysis (Ref. 21) to more detailed numerical evaluation. The seed parallel Reynolds stress induced by turbulence is defined by $\Re_\parallel \equiv \langle \tilde{\mathbf{u}}_r \tilde{\mathbf{u}}_\parallel \rangle$, where $\tilde{\mathbf{u}}_r$ is the radial component of the fluctuating $\mathbf{E} \times \mathbf{B}$ velocity, $\tilde{\mathbf{u}}_\parallel$ is the fluctuating parallel flow velocity, and $\langle \cdots \rangle$ stands for the ensemble average. For tokamaks, the physical quantity is the average over a magnetic surface,

$$\Re_\parallel \equiv \frac{1}{2\pi} \int_{-\pi}^{\pi} d\vartheta \langle \tilde{\mathbf{u}}_r \tilde{\mathbf{u}}_\parallel \rangle. \tag{33}$$

In the fluid ITG model, $\tilde{\mathbf{u}}_r$ and $\tilde{\mathbf{u}}_\parallel$ are, respectively, expressed by

$$\tilde{\mathbf{u}}_r = -\frac{T_e}{eBr} \frac{\partial \varphi}{\partial \vartheta}, \tag{34}$$

$$\tilde{\mathbf{u}}_\parallel = -\frac{iT_e}{m_i} \frac{1}{\omega} \left(1 + \frac{\omega_{*i}}{\omega}\right) \nabla_\parallel \varphi, \tag{35}$$

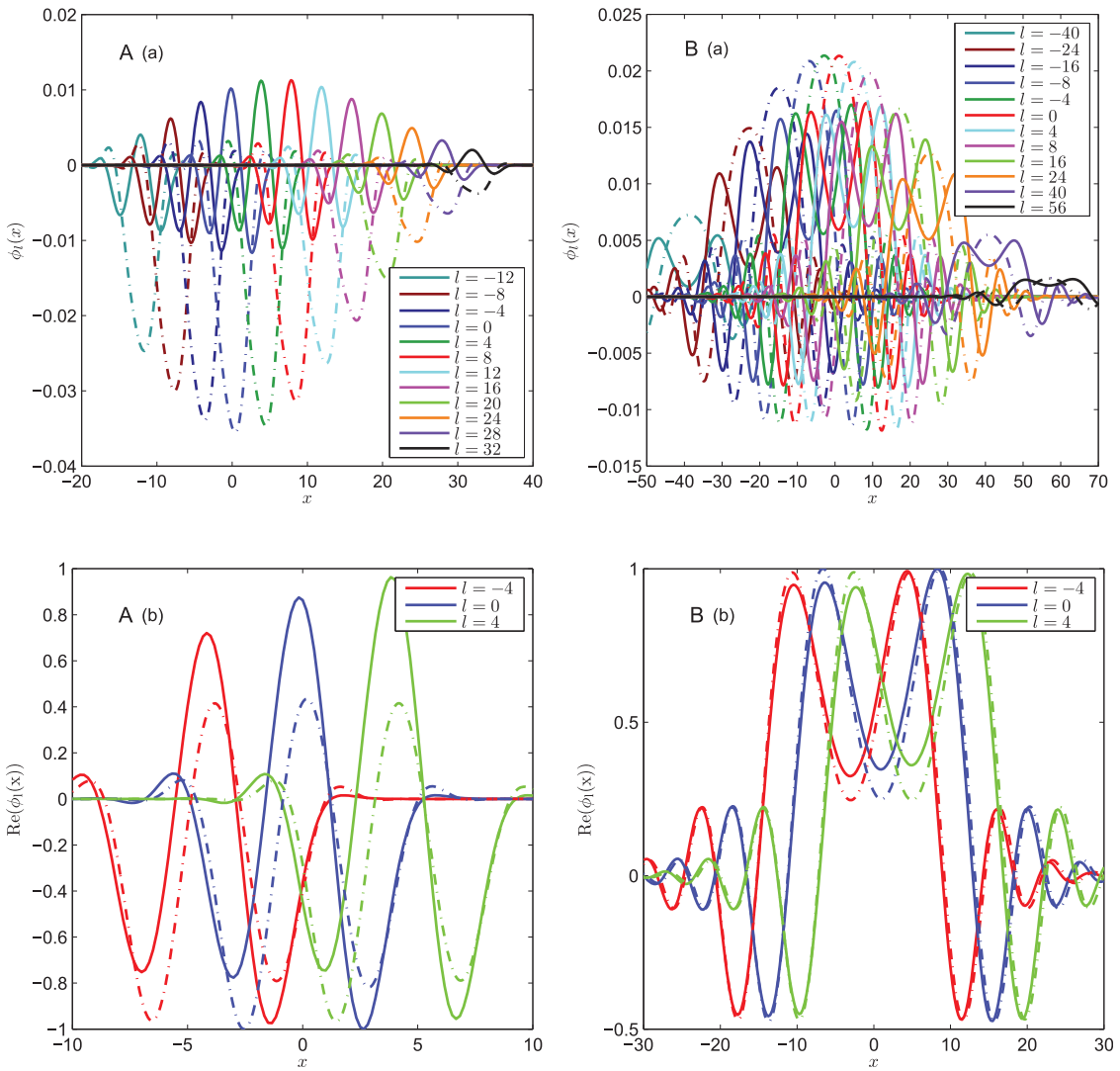

FIG. 4. (a) the real (solid line) and imaginary (dotted-dashed line) parts of 2-D wave function $\varphi_l(x)$ versus x for various l for parameter sets A and B; (b) the comparison of real parts of $\varphi_l(x)$ between numerical solutions (solid line) and analytical ones (dotted-dashed line) obtained from Eq. (B6) for several selected sidebands for parameter sets A and B.

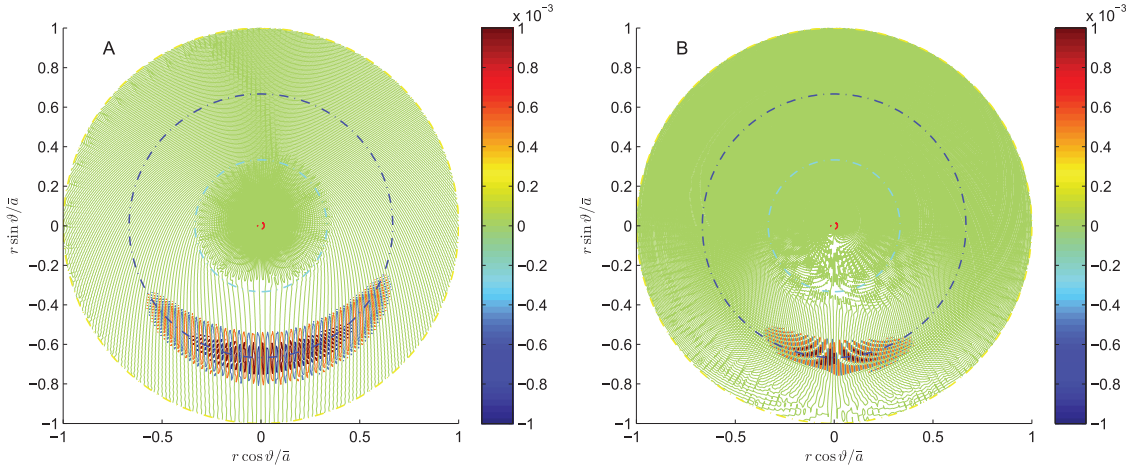

FIG. 5. The potential contours of the real parts of 2-D mode structure on a poloidal cross section for parameter sets A and B. $\bar{a}$ equals $3r_0/2$ in this figure.

where, φ is the normalized (to T_e/e) fluctuating electrostatic potential. Substituting Eqs. (34) and (35) into Eq. (33) yields the contribution from the jth rational surface to $\Re_\parallel$

$$\Re_{\parallel,j} = -\frac{T_e^2}{2m_i eB}\mathrm{Im}\left[\frac{1}{\omega}\left(1+\frac{\omega_{*i}}{\omega}\right)\right]\sum_{l=-\infty}^{\infty}\frac{m+l}{r}k_\parallel|\varphi_l(x)|^2\mathbf{e}_r\mathbf{b}, \tag{36}$$

where, $k_\parallel \equiv (x-l)/qR$, $\mathbf{e}_r$, and $\mathbf{b}$ are the unit vectors in the radial and magnetic field directions, respectively. The total stress is obtained by summing over all the rational surfaces. Under the approximation[15]

$$\sum_j \Re_{\parallel,j} \approx \int_{-\infty}^{\infty} dx \Re_{\parallel,j}, \tag{37}$$

it yields

$$\Re_\parallel = \sum_j \Re_{\parallel,j} \approx -\frac{k_\vartheta T_e^2}{2m_i eB}\mathrm{Im}\left[\frac{1}{\omega}\left(1+\frac{\omega_{*i}}{\omega}\right)\right]\langle k_\parallel\rangle\int_{-\infty}^{\infty}dx\sum_{l=-\infty}^{\infty}|\varphi_l(x)|^2\mathbf{e}_r\mathbf{b}, \tag{38}$$

where $\langle k_\parallel\rangle$ is a measure of the seed parallel Reynolds stress and is defined by

$$\langle k_\parallel\rangle \equiv \frac{\sum_{l=-\infty}^{\infty}\int_{-\infty}^{\infty}dx\varphi_l^* k_\parallel\varphi_l}{\sum_{l=-\infty}^{\infty}\int_{-\infty}^{\infty}dx\varphi_l^*\varphi_l}. \tag{39}$$

Equation (38) is essentially same as the last two terms of Eq. (5) in Ref. 31.

Note that the analytical expression for $\overline{\chi}$ seen in Eq. (27) suggests that it is the finite radial shift from rational surface (non-zero k_*) that is the source of finite $\langle k_\parallel\rangle$.

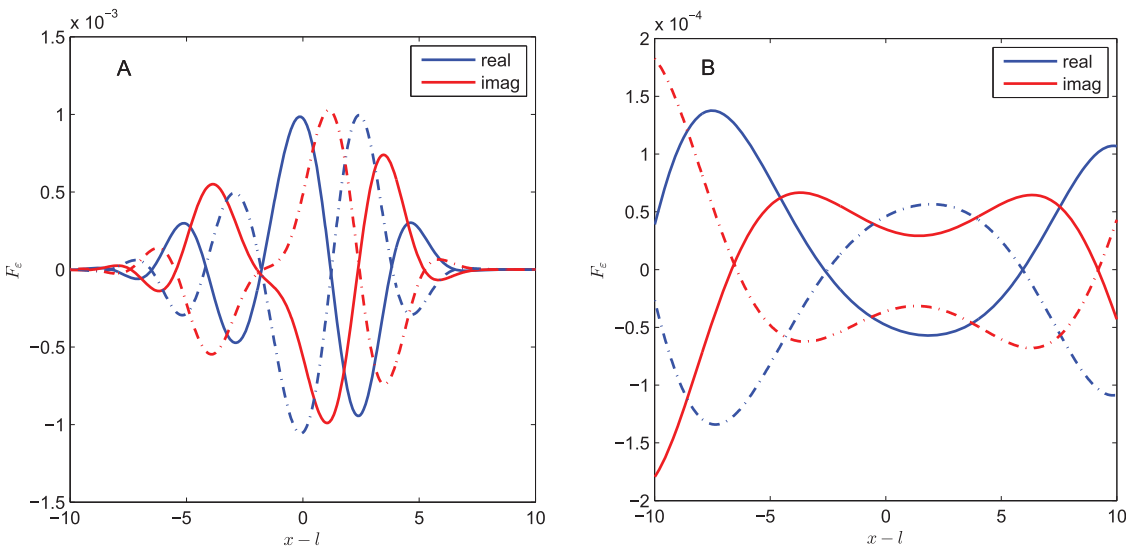

FIG. 6. The fitness of the ballooning solution to the 2-D model equation in the (x, l) representation for parameter sets A and B. Solid line: $l=0$; dotted-dashed line: $l=10$.

The analytical mode structure is obtained as a single component on the RHS of Eq. (29),

$$\varphi_l(x) = \sqrt{\frac{i}{n|\mu|\eta^2}} e^{ik_*(x-l)-i(x-l)^2/(2\eta^2)+i\sigma_\lambda\left[n\mu+l^2/(2n\mu)-l\pi/2\right]+i3\pi/4-i\vartheta_0/2}. \tag{40}$$

Substituting Eq. (40) into Eq. (39) and expressing $x-l$ of $k_\parallel$ in terms of parameter derivative $-d/d\beta$ yields

$$\langle k_\parallel \rangle = \frac{\sum_{l=-\infty}^{\infty} e^{-|\mathrm{Im}\mu|l^2/(n|\mu|^2)} \left(-\frac{d}{d\beta}\right) \int_{-\infty}^{\infty} dx e^{-(x-l)^2 \mathrm{Im}\eta^2/|\eta^2|^2-\beta(x-l)}}{qR \sum_{l=-\infty}^{\infty} e^{-|\mathrm{Im}\mu|l^2/(n|\mu|^2)} \int_{-\infty}^{\infty} dx e^{-(x-l)^2 \mathrm{Im}\eta^2/|\eta^2|^2-\beta(x-l)}}, \tag{41}$$

where $\beta \equiv 2\mathrm{Im}k_*$. The operator $-d/d\beta$ yields the quantity independent of l. The absolute sign of Im μ arises from the localization rule (see footnote b). Therefore, Eq. (41) is reduced to

$$\langle k_\parallel \rangle = -\frac{1}{qR}|\eta^2|^2 \frac{\mathrm{Im}(k_*)}{\mathrm{Im}(\eta^2)} \tag{42}$$

and k_* is solved (from Eq. (25) for small $|q/\hat{s}\eta^2| \ll 1$) to be

$$k_* \approx \sigma_\lambda \frac{(\hat{s}-1)q}{\hat{s}\eta^2}. \tag{43}$$

Combining Eqs. (42) and (43), we find

$$\langle k_\parallel \rangle = \sigma_\lambda \frac{(\hat{s}-1)}{\hat{s}R}. \tag{44}$$

This expression for $\langle k_\parallel \rangle$ *including all sidebands is the same as that of Ref.* 21*; the latter was obtained for* $l \to 0$ *only*. The semi-numerical $\langle k_\parallel \rangle$ is computed in terms of the 2-D ballooning solution by making use of the formula

$$\langle k_\parallel \rangle \approx \frac{\int_{-\infty}^{\infty} dk \chi^*(k, \sigma_\lambda\pi/2) i\frac{\partial}{\partial k}\chi(k, \sigma_\lambda\pi/2)}{qR\int_{-\infty}^{\infty} dk \chi^*(k, \sigma_\lambda\pi/2)\chi(k, \sigma_\lambda\pi/2)} \tag{45}$$

derived from Eq. (39) via the ballooning transform, and approximating the localized $\psi(\lambda)$ at $\sigma_\lambda\pi/2$ by δ-function. The significance of this computation is to get rid of the approximation caused by making use of analytic expression of ballooning solution Eq. (26). The numerical results in use of Eq. (45) are found in excellent agreement with 2-D integration in use of Eq. (39) for a few selected examples.

The dimensionless parallel wave number $\langle \hat{k}_\parallel \rangle = \langle k_\parallel \rangle R$ (normalized to major radius), obtained by various approaches (using Eqs. (42), (44), and (45)), is plotted and compared with the magnetic shear $\hat{s}$ in Fig. 7. For this exercise, we added another parameter set C in addition to the parameter sets A and B. The parameter set C is essentially the same as the parameter set A, but has a different density gradient, $\varepsilon_n = -0.3$ instead of $\varepsilon_n = -0.1$. The parameter set C is purposely chosen to violate the requirement $\eta^2 \gg 1$ needed for the validity of analytical expression Eq. (26). The three hollow circles in Fig. 7 correspond to the sets A, B, and C for which, $|\eta^2| = 2.72$, 24.5, and 1.31, respectively. It is very interesting to note that the simple analytic formula Eq. (44) is a good description for the sign reversal of $\langle \hat{k}_\parallel \rangle$ at $\hat{s} = 1$.

In recent years, a few laboratories have reported intrinsic toroidal rotation in tokamaks.[32–35] The spontaneous symmetry breaking induced parallel Reynolds stress is a ubiquitous turbulence driven mechanism for sowing seeds for the intrinsic toroidal rotation. This feature, however, is not unique to ITG and is common to all types of tokamak turbulence because of the 2-D mode structure imposed by the tokamak geometry.

One must, however, use extreme caution in applying the theoretical results (obtained in this paper) to the observations in experiment and simulation:

(1) First of all, the seed parallel Reynolds stress may not be directly proportional to the actual Reynolds stress in tokamaks. For example, the seed Reynolds stress drives initial shear flow, which in turn may drive other instabilities, or induce radial electric fields to achieve a new equilibrium. In the new equilibrium, the seed Reynolds stress may not be dominant.
(2) Second, the above calculation is model-dependent; it is based on ITG instability in a non-dissipative fluid, for which the normal density gradient is stabilizing. Other instabilities are likely to lead to different parametric tendencies.
(3) Last but not the least, the present theory is a simple illustrative model founded on only one symmetry breaking term. Many other contending symmetry breaking terms, such as those due to radial dependency and derivatives on the poloidal angle, are ignored without evaluating their weights. Nonetheless, there could be some interesting qualitative features shared among different models and different symmetry breaking terms. For example, the sign of Reynolds stress reverses at a certain radial

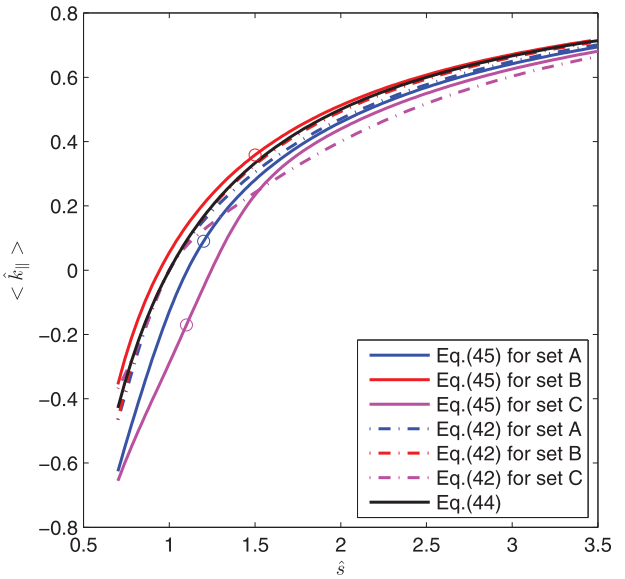

FIG. 7. Dimensionless parallel wave number $\langle \hat{k}_{\|} \rangle \equiv \langle k_{\|} \rangle R$ versus magnetic shear $\hat{s}$ for different parameter sets.

position. Many more concrete calculations are needed to supplement this effort.

V. CONCLUSION

In this paper, building on the work reported in Ref. 21, we have harnessed theoretical, numerical, and graphical methods to present the essence of the 2-D BM-II pertinent to a non-dissipative fluid ITG model. The primary result is a theory of induced toroidal rotations via spontaneous symmetry breaking. The resulting 2-D ballooning eigenmode equations are numerically solved for the localized BM-II; the solution comprises, *inter alia*, the global eigenvalue, the 2-D mode structure, and the seed parallel Reynolds stress under verified asymptotic conditions. The numerical solutions for all explored parameter regimes agree well with earlier theories of BM-II (Refs. 15, 16, and 21) under the assumption that $\Omega(\lambda)$ is truncated to the first harmonics. In that case, $\psi(\lambda)$ exhibits a monopole-like structure. It demonstrates the mechanism of (instability-induced) spontaneous symmetry breaking that leads to the formation of local modes.

The characteristic features of BM-II are summarized as follows. The mode structure is radially asymmetric and is localized at the poloidal angle $\vartheta = -\sigma_\lambda \pi/2$, where σ_λ is determined by the localization rule: $\sigma_\lambda = 1$ for Im $\mu < 0$ and $\sigma_\lambda = -1$ for Im $\mu > 0$. The measures of poloidal and radial localization are, respectively, $\bar{l} \equiv |\mu| \sqrt{n/|\mathrm{Im}\mu|} \ll m$ and $\Delta r/r_0 \equiv |\mu|/q\hat{s}\sqrt{n|\mathrm{Im}\mu|}$.

In addition, the accuracy of numerical solutions of the 2-D ballooning equation set is tested by substituting them back in the original equation in (x, l) representation via FFT. The numerical solutions turn out to be well within the assumed accuracy ($\sim 1/n$).

Finally, $\langle k_{\|} \rangle$, the key determinant of the seed parallel Reynolds stress, is derived in 2-D ballooning representation and computed numerically and found to be consistent with analytical solutions. It is important to note that the main result of the present theory on seed parallel Reynolds Stress is the demonstration of sign reversal when the magnetic shear parameter equals one. However, it must be stressed that more work needs to be done before one can, confidently, attempt to correlate and "meaningfully" compare the obtained results with experiments and simulations.

ACKNOWLEDGMENTS

This work was supported by National Magnetic Confinement Fusion Science Program (China) under Grant No: 2009GB101002 (TX), ITER-China Program No. 2010GB107000 National Natural Science Foundation of China (NSFC-11075162) (YZZ), and USDOE Contract No. DE–FG 03-96ER-54366 (SMM).

APPENDIX A: THE ITERATIVE PROCEDURE FOR GLOBAL EIGENVALUE OF BALLOONING THEORY

In this appendix, we provide the details of the iterative procedure for determining global eigenvalues in ballooning theory (Sec. III).

Specifically, the set of equations of Eqs. (14) and (17) is cast into the following form, where the λ-parameterization is explicitly shown, and λ_0 stands for the assumed λ localization. We shall solve the system iteratively.

$$\{L_0[\omega(\lambda_0), \lambda] - \Omega[\omega(\lambda_0), \lambda]\}\chi(k, \lambda; \omega(\lambda_0)) = 0, \quad \text{(A1)}$$

$$\frac{i\bar{L}_1[\omega(\lambda_0), \lambda]}{n}\frac{d \ln \psi(\lambda)}{d\lambda} - \{\Omega[\omega] - \Omega[\omega(\lambda_0), \lambda]\} = 0, \quad \text{(A2)}$$

where, $\Omega[\omega]$ is the global eigenvalue,

$$L_0[\omega(\lambda_0), \lambda] = \frac{1}{\eta^2(\omega(\lambda_0))}\frac{\partial^2}{\partial k^2} + \eta^2(\omega(\lambda_0))k^2 - \frac{2q}{\hat{s}}[\cos(k+\lambda) + k\hat{s}\sin(k+\lambda)], \quad \text{(A3)}$$

$$\bar{L}_1[\omega(\lambda_0), \lambda] = \frac{1}{\hat{s}\varepsilon_n}\frac{\omega_{*i}}{\omega_{*e}}\frac{1 + (k_\vartheta \rho_s)^2 + \omega_{*i}\left[(k_\vartheta \rho_s)^2 - \omega_{*e}/\omega_{*i}\right]/\omega(\lambda_0)}{[1 + \omega_{*i}/\omega(\lambda_0)]^2}, \quad \text{(A4)}$$

$$\Omega[\omega(\lambda_0), \lambda] = -\frac{q}{\hat{s}\varepsilon_n}\frac{\omega(\lambda)}{\omega_{*e}}\frac{1 + (k_\vartheta \rho_s)^2 + \omega_{*i}\left[(k_\vartheta \rho_s)^2 - \omega_{*e}/\omega_{*i}\right]/\omega(\lambda_0)}{1 + \omega_{*i}/\omega(\lambda_0)}. \quad \text{(A5)}$$

Notice that the definitions of Eqs. (A3)–(A5) are different from those of Eqs. (11)–(13) because of the explicit λ-parameterization. On the other hand, it is worth pointing out the term "global eigenvalue" in contrast to "local eigenvalue." The latter would refer to the one corresponding to the 1-D ballooning equation (Eqs. (A1), (A3), and (A5)) with λ_0 replaced by λ.

In practice of iterative solution, the initial guess can be obtained in *ad hoc* manner. For example, for a given set of parameters, one may use a working parameter running from zero to one in front of the curvature term of Eq. (A3), while setting $\lambda_0 = \sigma_\lambda \pi/2$ in that term. This way assures using the correct ITG branch of slab model to begin with. We substitute initial guess $\omega^{(0)}$ (the localized solution near $\lambda_0 = \sigma_\lambda \pi/2$) into $L_0[\omega, \lambda]$ and solve the ballooning equation,

$$\left\{L_0\left[\omega^{(0)}, \lambda\right] - \Omega^{(0)}[\lambda]\right\}\chi^{(0)}(k, \lambda) = 0, \tag{A6}$$

where, $\Omega^{(0)}[\lambda]$ is the solved eigenvalue as a function of λ. Notice that in Eq. (A6), the λ dependence arises solely from the mode coupling effects contained in the curvature term. The same $\omega^{(0)}$ is also substituted into Eq. (A4) for $\omega(\lambda_0)$ in $\overline{L}_1[\omega(\lambda_0), \lambda]$. Now, Eq. (A2) becomes

$$\frac{i\overline{L}_1[\omega(\lambda_0), \lambda]}{n}\frac{d\ln\psi^{(0)}(\lambda)}{d\lambda} - \left\{\Omega[\omega] - \Omega^{(0)}[\lambda]\right\} = 0. \tag{A7}$$

In general, $\overline{L}_1$ could weakly depend on λ. This causes only minor quantitative correction to our numerical results. Integrating over λ on the period yields the first iterative global eigenvalue

$$\Omega^{(1)}\left[\omega^{(1)}\right] = \frac{\int_{-\pi}^{\pi}\frac{d\lambda}{\overline{L}_1[\omega(\lambda_0), \lambda]}\Omega^{(0)}[\lambda]}{\int_{-\pi}^{\pi}\frac{d\lambda}{\overline{L}_1[\omega(\lambda_0), \lambda]}}, \tag{A8}$$

where corresponding $\omega^{(1)}$ is to be solved from Eq. (A5), as soon as the RHS of Eq. (A8) is computed. This $\omega^{(1)}$ is used to kick off the next iteration by substituting it into $L_0[\omega(\lambda_0), \lambda]$ and $\overline{L}_1[\omega(\lambda_0), \lambda]$ for $\omega(\lambda_0)$, respectively. For the ith iteration, the accuracy of the solution can be measured by

$$\delta^{(i)} \equiv \left|1 - \frac{\omega^{(i)}}{\omega^{(i+1)}}\right|. \tag{A9}$$

The success of the iteration relies on the fast convergence to make $\delta^{(i)}$ reach a sufficiently small value. Up to the date, we have accomplished dozens of groups of parameters by using the iterative method. The results indeed show the success. Typically, the iteration number is 4 to achieve $\delta < 10^{-4}$ for such parameters as $k_\vartheta \rho_s = 0.6$, $\hat{s} = 1.2$, $q = 1.5$, $\varepsilon_n = -0.1$, $\omega_{*i}/\omega_{*e} = 3$, and $n = 60$.

APPENDIX B: ANALYTICAL SOLUTION OF BALLOONING EQUATIONS FOR ARBITRARY λ

For arbitrary λ, the ballooning equation, in lieu of Eq. (24) for $\lambda \to \lambda_0 = \sigma_\lambda \pi/2$, is

$$\left\{\frac{1}{\eta^2}\frac{\partial^2}{\partial k^2} + V(k, \lambda) - \Omega(\lambda)\right\}\chi(k, \lambda) = 0, \tag{B1}$$

where

$$V(k, \lambda) = \eta^2 k^2 - \frac{2q}{\hat{s}}[\cos(k + \lambda) + k\hat{s}\,\sin(k + \lambda)]. \tag{B2}$$

Expanding $V(k, \lambda)$ at $k_*(\lambda)$ defined by $\partial V(k, \lambda)/\partial k = 0$, we obtain

$$k_* = \frac{q}{\eta^2\hat{s}}[(\hat{s} - 1)\sin(k_* + \lambda) + k_*\hat{s}\cos(k_* + \lambda)]. \tag{B3}$$

The corresponding analytical solution of the ballooning equation, Eq. (B1), still keeps the form of Eq. (26), but replacing k_* by $k_*(\lambda)$, the solution of Eq. (B3), i.e.,

$$\chi(k, \lambda) = e^{i\eta^2(k - k_*(\lambda))^2/2}. \tag{B4}$$

In the physical space, Eq. (B4), corresponding to Eq. (27), reads

$$\overline{\chi}(x - l, \lambda) = \sqrt{\frac{2\pi i}{\eta^2}}e^{ik_*(\lambda)(x-l) - i(x-l)^2/(2\eta^2)}. \tag{B5}$$

This expression combined with Eq. (20) is used to calculate the analytical 2-D mode structure

$$\varphi_l(x) = \frac{1}{2\pi}\int_{-\pi}^{\pi} d\lambda\overline{\chi}(x - l, \lambda)\psi(\lambda)e^{-i\lambda l}. \tag{B6}$$

[1] J. W. Connor, R. J. Hastie, and J. B. Taylor, Phys. Rev. Lett. **40**, 396 (1978).
[2] Y. C. Lee and J. W. Van Dam, in *proceedings of the Finite Beta Theory Workshop, Varenna Summer School of Plasma Physics, September 1977, Varenna, Italy*, edited by B. Coppi and B. Sadowski (U.S. Department of Energy, Office of Fusion Energy, Washington DC, 1979), CONF-7709167, p. 93.
[3] J. W. Connor, R. J. Hastie, and J. B. Taylor, Proc. R. Soc. London, Ser. A **365**, 1 (1979).
[4] J. Wesson, *Tokamaks*, 3rd ed. (Oxford University Press, Clarendon, UK, 2004), Sec. 8.5, p. 441.
[5] Y. Z. Zhang and S. M. Mahajan, Phys. Lett. A **157**, 133 (1991).
[6] Y. Z. Zhang, S. M. Mahajan, and X. D. Zhang, Phys. Fluids B **4**, 2729 (1992).
[7] R. L. Dewar, J. Manickam, R. C. Grimm, and M. S. Chance, Nucl. Fusion **21**, 493 (1981).
[8] R. L. Dewar, "Theory of fusion plasma," in *Proceedings of the Workshop Held at Villa Cipressi-Varenna, Italy, 24-28 August 1987*, edited by A. Bondeson, E. Sindoni, and F. Troyon (Editrice Compositori Societa Italiana di Fisica, Bologna, Italy, 1988), p. 107.
[9] R. L. Dewar and Y. Z. Zhang, Bull. Am. Phys. Soc. **37**, 1436 (1992).
[10] X. D. Zhang, Y. Z. Zhang, and S. M. Mahajan, Phys. Fluids B **5**, 1257 (1993).
[11] J. W. Connor, J. B. Taylor, and H. R. Wilson, Phys. Rev. Lett. **70**, 1803 (1993).
[12] J. B. Taylor, J. W. Connor, and H. R. Wilson, Plasma Phys. Controlled Fusion **35**, 1063 (1993).
[13] X. D. Zhang, Y. Z. Zhang, and S. M. Mahajan, Phys. Plasma **1**, 381 (1994).
[14] R. L. Dewar, Y. Z. Zhang, and S. M. Mahajan, Phys. Rev. Lett. **74**, 4563 (1995).
[15] Y. Z. Zhang and S. M. Mahajan, Phys. Plasma **2**, 4236 (1995).
[16] J. B. Taylor, H. R. Wilson, and J. W. Connor, Plasma Phys. Controlled Fusion **38**, 243 (1996).

[17]F. Zonca and L. Chen, Phys. Rev. Lett. **68**, 592 (1992).
[18]F. Zonca and L. Chen, Phys. Fluids B **5**, 3668 (1993).
[19]M. N. Rosenbluth, H. L. Berk, J. W. Van Dam, and D. M. Lindberg, Phys. Rev. Lett. **68**, 596 (1992).
[20]M. N. Rosenbluth, H. L. Berk, J. W. Van Dam, and D. M. Lindberg, Phys. Fluids B **4**, 2189 (1992).
[21]Y. Z. Zhang, Nucl. Fusion Plasma Phys. **30**, 193 (2010) (in Chinese with English abstract).
[22]P. H. Diamond, C. J. McDevitt, and Ö. D. Gürcan, Phys. Plasma **15**, 012303 (2008).
[23]C. J. McDevitt, P. H. Diamond, Ö. D. Gürcan, and T. S. Hahm, Phys. Rev. Lett. **103**, 205003 (2009).
[24]P. H. Diamond, C. J. McDevitt, Ö. D. Gürcan, T. S. Hahm, W. X. Wang, E. S. Yoon, I. Holod, Z. Lin, V. Naulin, and R. Singh, Nucl. Fusion **49**, 045002 (2009).
[25]C. J. McDevitt, P. H. Diamond, Ö. D. Gürcan, and T. S. Hahm, Phys. Plasma **16**, 052302 (2009).
[26]Ö. D. Gürcan, P. H. Diamond, C. J. McDevitt, and T. S. Hahm, Phys. Plasma **17**, 032509 (2010).
[27]Y. Kosuga, P. H. Diamond, and Ö. D. Gürcan, Phys. Plasma **17**, 102313 (2010).
[28]Ö. D. Gürcan, P. H. Diamond, P. Hennequin, C. J. McDevitt, X. Garbet, and C. Bourdelle, Phys. Plasma **17**, 112309 (2010).
[29]R. Singh, R. Ganesh, R. Singh, P. Kaw, and A. Sen, Nucl. Fusion **51**, 013002 (2011).
[30]W. X. Wang, T. S. Hahm, S. Ethier, L. E. Zakharov, and P. H. Diamond, Phys. Rev. Lett. **106**, 085001 (2011).
[31]Ö. D. Gürcan, P. H. Diamond, T. S. Hahm, and R. Singh, Phys. Plasma **14**, 042306 (2007).
[32]J. E. Rice, A. Ince-Cushman, J. S. deGrassie, L.-G. Eriksson, Y. Sakamoto, A. Scarabosio, A. Bortolon, K. H. Burrell, B. P. Duval, C. Fenzi-Bonizec, M. J. Greenwald, R. J. Groebner, G. T. Hoang, Y. Koide, E. S. Marmar, A. Pochelon, and Y. Podpaly, Nucl. Fusion **47**, 1618 (2007).
[33]M. Yoshida, Y. Kamada, H. Takenaga, Y. Sakamoto, H. Urano, N. Oyama, G. Matsunaga, and JT-60 Team, Phys. Rev. Lett. **100**, 105002 (2008).
[34]N. Oyama and JT-60 Team, Nucl. Fusion **49**, 104007 (2009).
[35]J. E. Rice, J. W. Hughes, P. H. Diamond, Y. Kosuga, Y. A. Podpaly, M. L. Reinke, M. J. Greenwald, Ö. D. Gürcan, T. S. Hahm, A. E. Hubbard, E. S. Marmar, C. J. McDevitt, and D. G. Whyte, Phys. Rev. Lett. **106**, 215001 (2011).
[36]W. Horton, Jr., R. Estes, H. Kwak, and D.-I. Choi, Phys. Fluids **21**, 1366 (1978).
[37]R. J. Hastie, K. W. Hesketh, and J. B. Taylor, Nucl. Fusion **19**, 1223 (1979).